Enhanced Sorption of Radionuclides by Defect-Rich Graphene Oxide

Boulanger, N.; Kuzenkova, A. S.; Iakunkov, A.; Romanchuk, A. Y.; Trigub, A. L.; Egorov, A. V.; Bauters, S.; Amidani, L.; Retegan, M.; Kvashnina, K.; Kalmykov, S. N.; Talyzin, A. V.;

Originally published:

September 2020

ACS Applied Materials and Interfaces 12(2020)40, 45122-45135

DOI: https://doi.org/10.1021/acsami.0c11122

Defect- rich graphene oxide for enhanced sorption of radionuclides.

Nicolas Boulanger,[1] Anastasiia S. Kuzenkova[2], Artem Iakunkov[1], Anna Yu. Romanchuk[2], Alexander L. Trigub[2,3], Alexander V. Egorov[2], Stephen Bauters[4,5], Lucia Amidani[4,5], Marius Retegan[6], Kristina O. Kvashnina[4,5,2], Stepan N. Kalmykov[2,*] Alexandr V. Talyzin[1*]

[1] – Department of Physics, Umeå University, S-90187, Umeå, Sweden.

[2] - Department of Chemistry, Lomonosov Moscow State University, Leninskie Gory, Moscow 119991, Russia.

[3] - National Research Centre "Kurchatov Institute", Moscow, Russia

[4] - The Rossendorf Beamline at ESRF – The European Synchrotron, CS40220, 38043 Grenoble Cedex 9, France

[5] - Helmholtz Zentrum Dresden-Rossendorf (HZDR), Institute of Resource Ecology, PO Box 510119, 01314, Dresden

[6] - The European Synchrotron, CS40220, 38043 Grenoble Cedex 9, France

KEYWORDS graphene oxide, sorption, radionuclides, uranium, defects

ABSTRACT: Extremely defect graphene oxide (dGO) is proposed as an advanced sorbent for treatment of radioactive waste and contaminated natural waters. dGO prepared using a modified Hummers oxidation procedure, starting from reduced graphene oxide (rGO) as a precursor, shows significantly higher sorption of U(VI), Am(III) and Eu(III) compared to standard graphene oxides (GO). Earlier studies revealed the mechanism of radionuclide sorption related to defects in GO sheets. Therefore, explosive thermal exfoliation of graphite oxide was used to prepare rGO with large number of defects and holes. Defects and holes are additionally introduced by Hummers oxidation of rGO thus providing extremely defect-rich material. Analysis of characterization by XPS, TGA, FTIR shows that dGO oxygen functionalization is predominantly related to defects, such as flake edges and edge atoms of holes, whereas standard GO exhibits oxygen functional groups mostly on the planar surface. The high abundance of defects in dGO results in a 15-fold increase in sorption capacity of U(VI) compared to standard Hummers GO. The improved sorption capacity of dGO is related to abundant carboxylic groups attached hole edge atoms of GO flakes as revealed by synchrotron-based extended X-ray absorption fine structure (EXAFS) and high-energy resolution fluorescence detected X-Ray absorption near edge structure (HERFD-XANES) spectroscopy.

1. INTRODUCTION

Graphene oxide (GO) has been considered as an extremely promising material for treatment of radioactive waste and contaminated natural waters due to high capacity in sorption of radionuclides.[1-3] The processing of radioactive wastes aims on converting it into forms convenient for long-term storage or permanent disposal. Many sorbent materials have been studied for capture of radionuclides including zeolites,[4, 5] cement-based materials,[6, 7] clays [8-11] and carbon materials[12-15]. GO as a true 2D material has a high theoretical specific surface area which is important for efficient sorbent materials.[16] GO can be easily dispersed in water, exhibiting an experimental surface area determined by sorption of various molecules on the level 700-800 m^2/g[16, 17] with the theoretical surface value as high as 2600 m^2/g for a single layered sheet.[18] The high sorption ability of GO towards various cations of radionuclides and heavy metals has been demonstrated in several independent studies.[1, 3, 19-25] The mechanism of radionuclides sorption by GO has been a subject of intense discussions over past years.[26] It is clear that understanding the chemistry behind the cation-GO interaction is extremely important for the design of a new generation of even more efficient sorbent materials.[27] Tuning the properties of GO using different synthesis procedures and post preparation modifications provides possibilities for the further increase of GO sorption capacity.[2]

Graphite oxides are synthesized by strong oxidation of graphite, most commonly using Hummers[28] or Brodie[29] oxidation methods. Graphene oxide is easily produced using mild sonication of graphite oxides in water. Many variations of the Hummers procedure have also been proposed to make dispersion of graphite oxides in water even more efficient.[30] Properties of graphite oxides are significantly dependent on the method of preparation, e.g. thermal exfoliation temperatures,[31, 32] swelling,[33-36] mechanical strength of individual flakes,[37] sorption of polar solvents[38] and sorption capacity towards radionuclides.[2] In fact, GO's are a family of materials with strong variation in both degree of oxidation and relative numbers of various oxygen functional groups.[39,

[40] Moreover, the composition of GO is affected by ageing effects when stored on air.[41-43] In general for all types of GO, the planar surface of GO is functionalized mostly with epoxy and hydroxyl groups while the edges of GO flakes are predominantly terminated by carbonyls and carboxylic groups.[44] Recent studies demonstrated that the defects in GO sheets are not only always present and often abundant,[45, 46] but the defects (holes and vacancies) are responsible for some properties important for various applications.[47, 48]

Our earlier study revealed that GO prepared using Hummers oxidation (HGO) and Tour variation of Hummers method provides a higher capacity for sorption of radionuclides compared to GO synthesized by Brodie method (BGO).[2] BGO has fewer defects, higher relative amount of hydroxyl groups and more homogeneous distribution of functional groups over its surface.[33] HGO shows a relatively high percentage of carbonyl and carboxyl groups with a significant number of holes in the flakes and a strong disruption of the graphene structure.[33] Therefore, enhanced sorption properties of HGO towards several radionuclides have being assigned to interactions with carboxylic groups on GO flakes.[2] Preferential interaction of metal cations with carboxylic groups is in agreement with independent studies.[27, 49] Moreover, theoretical modelling, synchrotron radiation high-energy resolution fluorescence detected X-Ray absorption near edge structure (HERFD-XANES) and extended X-ray absorption fine structure (EXAFS) data on local coordination of sorbed radionuclide atoms provided evidence for sorption predominantly inside of small holes and vacancy defects of GO sheets.[2]

It should be noted that standard synthesis of GO is usually optimized for preparation of materials with minimal number of defects, aiming mostly on converting it into defect free graphene.[37, 50-52] Here we propose to use extremely defect-rich GO for efficient sorption of radionuclides from aqueous solutions. Precursor HGO was explosively exfoliated to produce defect rGO.[53] The rGO was then oxidized using a mild Hummers procedure which results in the formation of defect GO (dGO) with an abnormally high fraction of defects and functional groups with double bonded oxygen. Thanks to the very high number of defects and carboxylic groups, dGO shows strongly enhanced sorption of radionuclides.

2. EXPERIMENTAL SECTION

Starting materials. Graphite oxide was purchased from Abalonyx (product 1.8, CAS 1034343-98-0). According to the provider, the GO material was prepared using a slightly modified Hummers method. The characterization by XPS, XRD and FTIR confirmed that the material is standard HGO. According to our own characterization the GO confirms that all properties of this material are typical for standard HGO. Sodium nitrate was bought from Scharlab (CAS 7631-99-4), sulfuric acid was purchased from Merck (95 – 97 % concentration, CAS 7664-93-9). Potassium permanganate (CAS 7722-64-7), hydrogen peroxide (30 % concentration, CAS 7722-84-1) and hydrochloric acid (37 % concentration, CAS 7647-01-0) were all purchased from VWR Chemicals. The methylene blue used for characterization was bought from Sigma-Aldrich (CAS 122965-43-9). Reference sample of porous templated carbon with BET surface area of ~2000 m^2/g was purchased from ACS Material.

Synthesis of dGO. GO powder was thermally exfoliated in a large volume aluminium container. The container was rapidly inserted into a furnace heated to 240°C and removed after 6 minutes. Rapid heating results in the explosion of GO powder and formation of rGO powder. The thermal profile selected for the preparation of rGO provides maximal BET surface area according to earlier studies.[53] rGO powder was used as a precursor for the oxidation using standard Hummers procedure but with adjusted proportions between reagents.

For the synthesis of dGO typically 1 g of sodium nitrate was added into 40 mL sulfuric acid while stirring. 1 g of rGO was then added and the whole container placed into an ice bath while stirring. Next, 1 g of potassium permanganate was slowly added to the mixture with frequent controls of the suspension temperature, keeping it below ~20°C as this is a very exothermic process. The example here cites the batch with rGO:$KMnO_4$ ratio of 1:1. Note that the first attempt to synthesise dGO was performed using 1:3 ratio and resulted in too strong oxidation (see results section for details). When all the potassium permanganate was added, the suspension was preserved by stirring for a total time of 2 hours counted after the first introduction of potassium permanganate.

The container was then placed in an oil bath heated at 30°C for 1 hour. The container was then placed back into the ice bath and 40 mL deionized water was very slowly added, as this too is a very exothermic process. The whole procedure occurred within a fume hood as strong fumes were generated during this step. Once the water was added to the suspension and the reaction seemed to stop, the container was placed back into the oil bath and maintained at 90°C for 15 minutes. The suspension was then taken out of the oil bath and placed at room temperature. 90 mL of 6 % hydrogen peroxide was then added and the mixture was left stirring overnight at room temperature.

Finally, the mixture was rinsed by first washing it with 10 % hydrochloric acid: the mixture was poured in centrifugation containers and mixed with the acid solution, well shaken and centrifuged (Allegra 64R Centrifuge, Beckman Coulter) at 10 000 rpm for 10 minutes. This washing process was repeated 6 times. Then, the remaining material was repeatedly washed with deionized water until the pH of the solution was around 4 to 5. The mixture was each time well shaken and centrifu-

gated at 20 000 rpm for 30 minutes. The product was vacuum filtered using 1µm PTFE membrane (Omnipore, ref JAWP04700) and freeze dried over a few days. The preparation of a batch using 9 g rGO resulted in 8.6 g dGO, which is a yield of 95.5 %.

Characterization. X-ray diffraction spectra for the powder samples were recorded using Cu-Kα radiation (X' Pert³ Powder diffractometer by PANalytical). Fourier Transform Infrared (FTIR) spectra were recorded for powder samples using a Brucker IFS 66 v spectrometer. Surface area of the different materials was determined by recording nitrogen sorption isotherms using an Autosorb iQ XR and Nova 1200e surface area and pore size analyzers (Quantachrome) at liquid nitrogen temperature. The relative pressure P/P_o for the BET plot was selected using a procedure optimized for microporous materials. Pore size volume and pore size distributions were determined using a slit-pore QSDFT equilibrium model.

Thermogravimetric analysis was performed using a Mettler Toledo TGA/DSC1 STAR^e System. The measurements were performed from room temperature up to 800°C at a heating rate of 5 K/min under a nitrogen flow of 50 mL/min.

XPS spectra were recorded with an Axis Ultra DLD spectrometer (Kratos Analytical Limited, Great Britain) using an Al-Kα radiation (hν = 1486.6 eV, 150 W). The pass energy of the analyzer was 160 eV for survey spectra and 40 eV for high resolution scans. A Kratos charge neutralizer system was used and the binding energy scale was adjusted with respect to the C1s line of aliphatic carbon set at 285.0 eV. All spectra were processed with the Kratos software.

Sorption measurements. Methylene Blue (MB) sorption measurements were performed using water solution of methylene blue and powders of tested materials using UV-vis method. Aqueous solution of methylene blue was added to solid powder material and stirred for 6 days. The concentration of MB and the proportion of solution to the amount of tested materials were selected to ensure that saturation sorption is achieved. Typically 1 mg/ml concentration of methylene blue and 0.5 mg/ml of tested material was used. The tested material was then removed by filtration and the concentration of the remaining solution was determined by UV-vis measurements using a Perkin Elmer Lambda 1050+ spectrometer. The UV-vis absorbance of MB at 664 nm was recorded to determine the remaining MB concentration in solution. Calibration of UV-vis absorbance was performed for a set of MB solutions with known concentrations.

Sorption experiments with radionuclides were carried out in plastic vials, as retention on the walls was found to be negligible. For the sorption experiments, an aliquot of the solution containing the radionuclides ^{241}Am, ^{152}Eu or ^{233,232}U was added to the GO suspension in 0.1 M $NaClO_4$ (experiments with each radionuclide were performed separately). A mixture of ^{233,232}U and natural uranium was used in order to vary the uranium concentration for isotherm experiments. In case of Eu isotherms solution of stable Eu(III) was used to make different total Eu concentration. The concentration of the solid phase in most of the experiments were 0.7 g/L, only in the cases of the pH-dependence of sorption on HGO it was equal to 0.07 g/L. The pH value was measured using a combined glass pH electrode (InLab Expert Pro, Mettler Toledo) with an ionomer (SevenEasy pH S20-K, Mettler Toledo) and was adjusted via addition of small amounts of dilute $HClO_4$ or NaOH. After equilibration, the GO suspension was centrifuged at 40000 g for 20 min (Allegra 64R, Beckman Coulter) to separate the solid phase from the solution. The sorption was calculated using the difference between the initial activity of the radionuclides and the activity measured in the solution after centrifugation. The activity of the radionuclides was measured using liquid-scintillation spectroscopy (Quantulus-1220, Perkin Elmer) and universal radiometric complex ORTEC DSPec50 (16013585).

For the purpose of EXAFS and FTIR characterization, samples equilibrated with only natural uranium were prepared. The concentration of the solid phase in this experiment was equal to 0.05 g/L with the total concentration of U(VI) kept at $1{\cdot}10^{-5}$ M. The pH values were c.a. 4.5-4.7.

EXAFS spectra were recorded at the Structural Materials Science beamline of the Kurchatov Synchrotron Radiation Source (Moscow, Russia) to analyse U local atomic environment. A storage ring with an electron beam energy of 2.5 GeV and a current of 80–100 mA was used. The X-ray beam was monochromatized using a Si(111) channel-cut monochromator, which provided an energy resolution of $\Delta E/E \approx 2 \times 10^{-4}$. Dumping of higher-energy harmonics was achieved by monochromator geometry distortion. EXAFS spectra of Zr foil were recorded for energy calibration. All experimental data were collected in transmission mode using ionization chambers filled with N_2 and Ar. Simultaneous acquisition of EXAFS data for the sample and reference was achieved by using three ionization chambers.

In this way, the monochromator energy calibration could be checked and corrected. At every energy point in the XANES region, the signal was integrated for 1 s, while in the case of EXAFS, integration time was set to 1 s at the beginning of the region and increased to 4 s at the end of the region. EXAFS data ($\chi_{exp}(k)$) were analyzed using the IFEFFIT data analysis package.[54] Standard procedures for the pre-edge subtraction and spline background removal were used for EXAFS data reduction. The radial pair distribution functions around the U ions were obtained by the Fourier transformation (FT) of the k^2-weighted EXAFS functions $\chi_{exp}(k)$ over the experimental ranges. Experimental spectra were fitted in R-space within range 1.2-4.2 Å. For the refined interatomic distances (R_i), the statistical error is 0.01–0.02 Å for the first coordination sphere.

ATR-FTIR spectra were recorded using a PLATINUM, a single reflection horizontal ATR accessory from Bruker Technologies, equipped with a diamond crystal. Ungrounded small species of the samples were analyzed at room temperature. For each sample, 256 scans were recorded under vacuum in the MIR region (4000-400 cm^{-1}) with a resolution of 4 cm^{-1}.

The U M_4 edge HERFD-XANES spectra were recorded at the ACT station of the CAT-ACT beamline of the KARA (Karlsruhe research accelerator) facility in Karlsruhe, Germany.[55] [56]A storage ring with an electron beam energy of 2.5 GeV and a current of 70–100 mA was used. The incoming X-ray beam was monochromatized by a Si (111) double crystal monochromator and slitted down to 500 x 500 µm at the sample position. The sample environment, including the entire Johann-type emission spectrometer, is contained within a He box to improve X-ray detectability and ensure sample stability. The samples were contained in the standard CAT-ACT pellet sample holder, using a double Kapton confinement of 8 and 12.5 µm thickness on the front side. To obtain the best possible resolution on the 5-crystal emission spectrometer, only 1 masked Si (220) crystal with bending radius 1 m was set at the U Mβ emission energy (3339.8 eV). Several continuous scan mode spectra were averaged to obtain the final results.

3. RESULTS AND DISCUSSION

3.1 Synthesis and characterization of dGO.

Extremely defect-rich GO was synthesised in our study using Hummers oxidation procedure applied to rGO precursor prepared using explosive thermal exfoliation of standard HGO.[53] Defects and holes in GO sheets are formed already during the synthesis by Hummers procedure.[45] Therefore, we suggested that reducing GO will keep these holes and after re-oxidation of rGO the number of holes will further increase.

It is well known that the result of Hummers oxidation depends very strongly on the type of precursor.[17, 31] Well crystalline graphite is typically used as a precursor for Hummers oxidation aimed on preparation of GO with lowest possible amount of defects. The idea of this study was to use rather defected rGO as a precursor for Hummers oxidation in order to prepare extremely defected GO.

Rapid thermal exfoliation of graphite oxide results in the formation of few layered rGO material with specific surface area (SSA) on the level 300-600 m^2/g depending on how rapidly the temperature is increased.[53] In contrast to chemical reduction of GO which preserves the graphene skeleton relatively intact, explosive thermal exfoliation provides larger numbers of defects in rGO sheets.[57, 58] It was argued already back in 60-s that holes and vacancies are formed due to rapid formation of gaseous carbon oxides and explosion driven by the build-up of gas pressure inside of graphite oxide interlayers.[17] Oxidation of defect rGO material was anticipated to result in GO material with many holes and vacancies per unit area thus increasing the number of edge carbons typically functionalized with carbonyl and carboxylic groups. The carboxylic groups inside the holes of dGO could be expected to serve as sorption sites for the removal of radioactive waste from aqueous solutions (Figure 1).

First attempt to oxidize rGO was performed using a Hummers procedure very similar to the one used for the preparation of standard HGO, with rGO:$KMnO_4$ proportion 1:3. However, when few layered and strongly defected rGO was used instead of graphite powder the oxidation proceeded too far. Most of the rGO powder was converted into dark brown solution with only very little dGO powder. The brown solution did not yield any precipitate even after using ultracentrifugation (~60 000 g for 4 hours and passed through finest filters (10 000 a.u.)). Some powdered material could be obtained from this solution by evaporation or using chem-

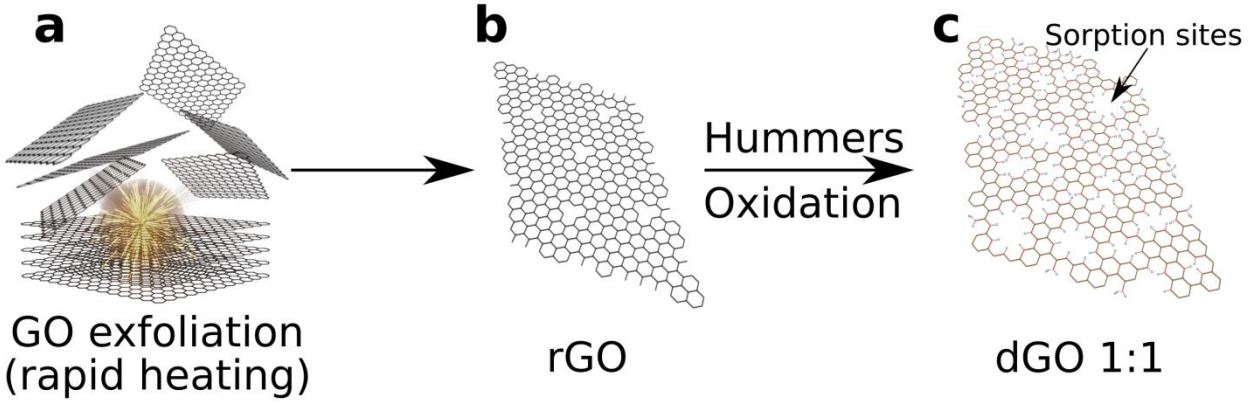

Figure 1. Scheme of defect GO preparation: a) explosive thermal exfoliation of HGO to produce rGO, b) using defect rGO for Hummers oxidation and c) formation of holey dGO with sorption sites on the holes edges.

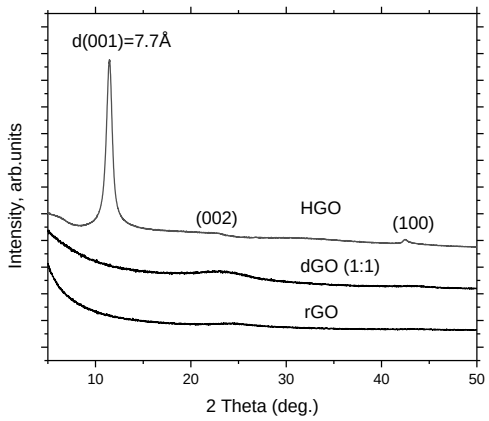

Figure 2. XRD patterns of HGO (intensity divided by ten), dGO (1:1) and precursor rGO. The pattern of HGO was scaled down in intensity.

ical precipitation by adding 10% NH_4Cl solution. These are not convenient methods for practical sorbent applications. It is obvious that extremely strong oxidation resulted in the breaking up of GO sheets into smaller and smaller fragments until some water soluble molecules were formed.

The difficulty to remove the dGO material from solution motivated us to use a milder oxidation procedure. The initial rGO:$KMnO_4$ 1:3 ratio was decreased to 1:1. This synthesis provided a sufficient amount of powdered material easily precipitated by centrifugation. In the following discussions, the two dGO materials will be named as dGO (1:1) and dGO (1:3) according to the proportion between carbon precursor and potassium permanganate. Most of the experiments were performed on dGO (1:1).

Characterization of dGO was performed using XRD, Raman and FTIR spectroscopies, analysis of N_2 sorption isotherms and XPS. Analysis of data, collected using combination of these methods, demonstrated that the material produced by re-oxidation of rGO is extremely defect rich GO.

Both dGO materials appeared to be amorphous in XRD tests yielding no (001) reflection, typical for standard HGO (Figure 2). The absence of a well aligned layered structure is expected for strongly defected GO sheets due to the large number of vacancies and holes disrupting the typical planar shape. The chemical composition and quantitative estimation for relative number of in-plane and edge carbon atoms can be evaluated using XPS data (Figure 3).

Table 1. XPS c1s data for HGO and dGO samples: C/O ratio and % of area (at.%) according to deconvolution of spectra shown in Figure 3. The value C/O=2.2 is calculated excluding oxygen from sulphate groups in standard HGO. No sulphur was detected in XPS spectra of dGO. The C=O peak includes contributions from carboxyl and carbonyl groups.

Sample	C/O	283.4-283.6 eV	285.0 eV (C-C)	286.6-286.8 eV (C-O)	288.9 eV (C=O)	290.5-291.0 eV
Precursor GO	1.95 (2.2)*	0.98	23.78	34.68	5.07	0.13
dGO 1:1	2.7	0.93	37.51	16.79	12.49	4.11
dGO 1:3	2.1	6.83	30.99	11.88	11.39	1.76

The most common interpretation of XPS spectra assigns C1s peaks of GO as following: 285.0 eV to C-C and C-OH groups, 286.6 eV to epoxy C-O-C groups and 288.9 eV to double bonded C=O, which includes carboxyls and carbonyls. Note that the C1s component due to hydroxyl groups is not resolved from C-C in XPS spectra, which makes overall quantitative analysis using only C1s deconvolution not reliable. However, it can confidently be concluded that dGO shows a strongly increased % of carboxyl/carbonyl functional groups compared to standard HGO. Formation of double bonded C=O is possible only on the edges of GO flakes or in vacancy defects. Formation of a large number of holes in GO flakes is expected also to result in a smaller relative number of functional groups located on planes. Indeed, dGO shows a much lower intensity of C1s component due to epoxy groups, which are attached to planar surface of flakes.

The significant difference between standard HGO and dGO is also confirmed by analysis of the O1s part of

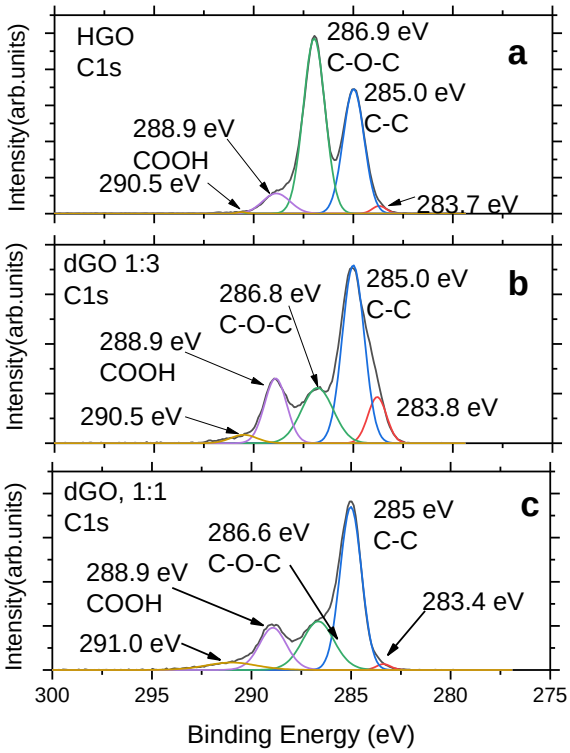

Figure 3. C1s XPS spectra of a) standard HGO, b) dGO (1:3) and c) dGO (1:1).

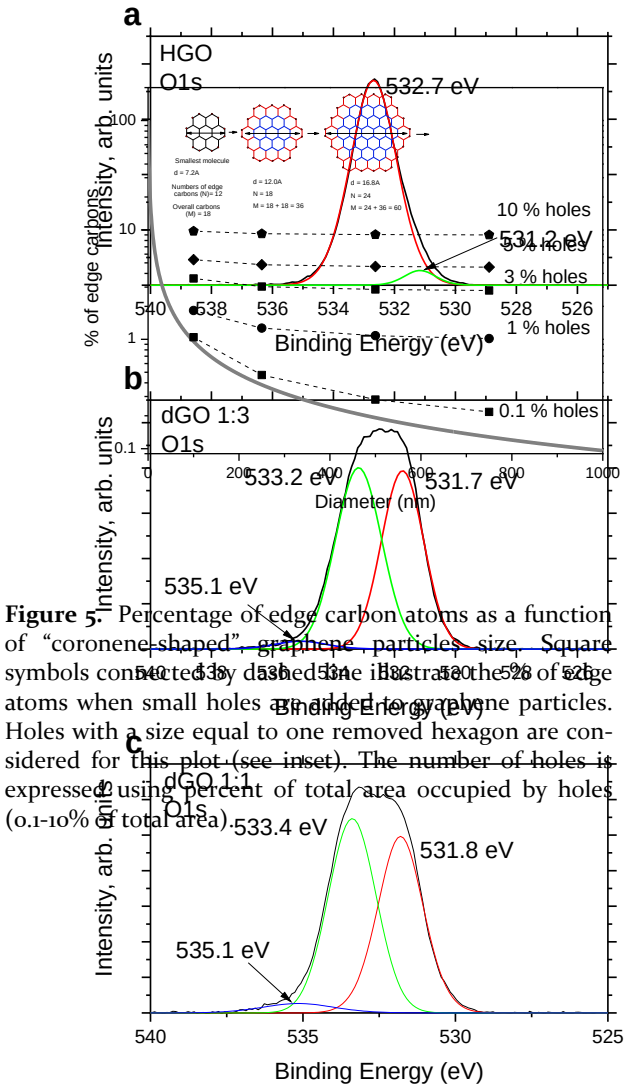

Figure 4. O1s XPS spectra of a) standard HGO, b) dGO (1:3) and c) dGO (1:1).

Figure 5. Percentage of edge carbon atoms as a function of "coronene-shaped" graphene particles size. Square symbols connected by dashed line illustrate the 2% of edge atoms when small holes are added to graphene particles. Holes with a size equal to one removed hexagon are considered for this plot (see inset). The number of holes is expressed using percent of total area occupied by holes (0.1-10% of total area).

XPS spectra (Figure 4). Standard HGO shows mostly one kind of oxygen with a major O1s peak at 532.7 eV,

which includes all oxygen attached to planes, and a rather minor component at 531.2 eV due to edge groups. The O1s spectra of dGO show two peaks with similar intensity, indicating that almost 50% of oxygen is in carboxyl and carbonyl groups attached to edges.

The very high percentage of edge carbons detected by XPS in dGO can be explained either by the very small size of flakes or by the large number of holes present. However, XPS does not allow to distinguish two kinds of edges: inner edges of holes and outer flake edges.

The possible relative amount of these two types of edge carbon atoms can be estimated using a simple model (Figure 5). Assuming the smallest graphene particle to be the size and shape of a coronene molecule, a set of progressively larger graphene particles of similar shape diameter (see inset in Figure 5) was considered and the percentage of edge atoms was plotted as a function of particle. It is clear that particles of irregular shape provide different proportions in the numbers of edge atoms to plane atoms. However, the plot shown in Figure 5 anyway provides a rough estimation for analysis of XPS data. Precursor GO material with 5 % of edge atoms placed only on the flake edges corresponds in this model to a particle size of only 20 nm in diameter. However, the particle size evaluated for the standard HGO material using AFM and SEM is in average about 300-500 nm, with some particles in micrometre size.[43] For dGO (~11% of edge carbons) the model provides diameters of particles as small as 8 nm. However, the contribution from carbon atoms located on the inner edges of holes needs also to be considered.

The relatively large percentage of carboxyl and carbonyl groups in HGO can be explained by assuming the existence of holes and point defects. It is clear that holes in GO sheets might have a variety of shapes and sizes, all affecting the proportion of edge atoms. As a simplified example we considered a hole in graphene sheet formed by removing 6 carbon atoms (one hexagon). This hole has 6 edge atoms and is large enough to accommodate 3 carboxylic and 3 carbonyl groups. The overall amount of holes is expressed using percent of area in holes relative to the total particle area. Assuming a realistic area of holes to be in the range of 1-10%, several points were added to the plot in Figure 5. Remarkably, a high % of edge carbon atoms inside of holes (e.g. ~10% similar to experimental value for dGO) can be achieved according to the model for any GO particle size assuming only 10% of total area to be in holes.

It should be noted that the direct experimental estimation of area covered by holes in GO sheets is very difficult even using High Resolution TEM. The GO is very sensitive to electron beam radiation and degrades immediately unless some very soft and very technically demanding conditions are implemented. Several studies where HRTEM of “graphene oxide” was presented, showed instead almost completely reduced graphene sheets. The best estimates using HRTEM that standard HGO has about 2% of area in holes with diameter less than 5 nm.[45] Using Figure 5 we can estimate that 2% of the area corresponds to approximately 4-5% of edge atoms for almost any reasonable GO flake size. This value of 4-5% edge atoms is in very good agreement with experimental XPS data for standard HGO (Figure 2 and Table 1).

The size of dGO (1:1) particles was analyzed using AFM and SEM. Most of the particles were found to be in the range 30-100 nm but few particles of larger size were also detected. Note that the particles tend to aggregate when precipitated and it is not always possible to distinguish individual particles from aggregates in SEM.

The oxidation degree of dGO determined by XPS is also confirmed using TGA data. The total weight loss over a temperature interval from ambient up to 700°C due to heating under nitrogen is about 55%, similar to standard HGO (~60%). However, standard HGO shows most of the weight loss in two sharp steps, firstly due to water desorption below 100°C (~8%, region I) and secondly due to the removal of oxygen functional groups from the planar surface around 150-240°C (~30%, region II).

Slow weight loss at temperatures above ~370°C (region III) is usually assigned to the removal of other oxygen groups (mostly carboxylic and carbonyls) attached to edges.

The TGA trace of dGO shows both steps typical for standard GO but only about 12% of weight is lost due to the removal of oxygen from the planar surface. The main weight loss (~24%) in dGO occurs gradually at temperatures above ~350°C (Figure 7). Therefore, TGA data are in agreement with the suggested extremely defected structure of dGO with a very large number of edge atoms and a decreased area of planar sheet surface. Thermal exfoliation of dGO results in formation of reduced dGO (rdGO) but without significant increase of BET surface area. HGO typically shows BET (N_2) surface area about 10-30 m^2/g which increases up to 300-500 m^2/g after rapid thermal exfoliation.[53, 59] The BET surface area of dGO remains almost unchanged after rapid thermal exfoliation thus providing additional arguments for the holey structure of dGO (Figure S1 in SI). The gases formed in a process of thermal deoxygenation are likely to escape easily through the defects of dGO sheets. As a result the gas pressure build-up which occurs in interlayers of standard HGO does not happen in dGO.

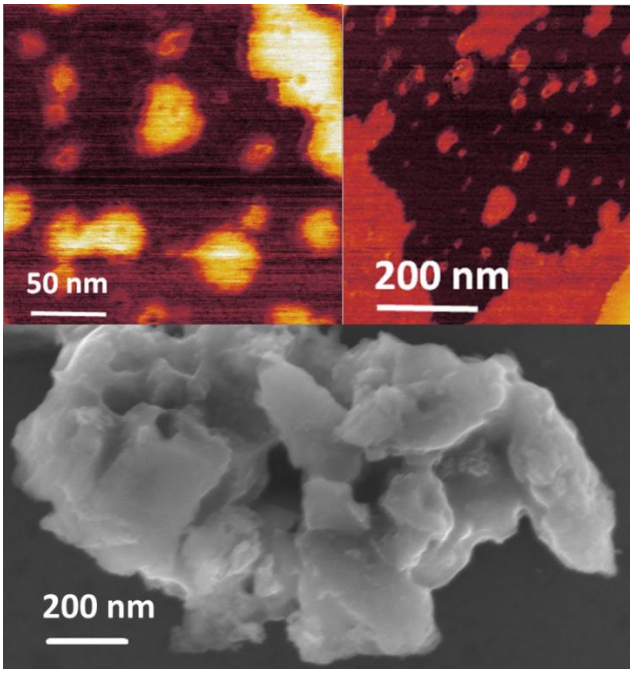

Figure 6. AFM (phase image) and SEM images of dGO (1:1).

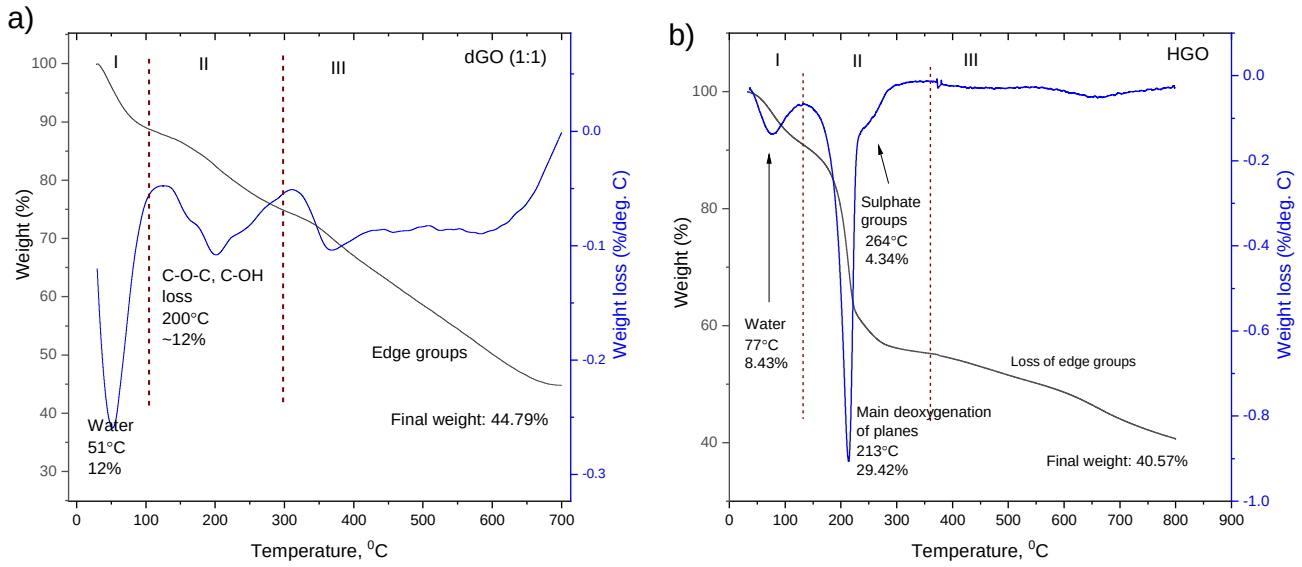

Figure 7. TGA traces of a) dGO (1:1) and b) precursor HGO.

Table 2. From left to right: BET surface area determined using analysis nitrogen sorption isotherms, saturated sorption of MB by HGO, BGO and dGO (1:1). The MB sorption does not correlate with the surface area determined using nitrogen sorption isotherms. Surface area estimated using MB sorption (2.54 m^2/mg) according to ref[16]

Sample	BET SSA (m^2/g)	Methylene blue sorption mg/g active material	Effective surface area m^2/g by MB sorption
HGO	<5	428	1086
BGO	<5	184	466
dGO (1:1)	19	879	2233
Porous Carbon	2007	586	1489

Defect structure is also in agreement with FTIR spectra of dGO shown in Figure 8. The spectra were recorded at vacuum conditions to minimize the amount of adsorbed water. The spectrum of precursor GO shows a peak from the C=C of graphene skeleton at 1565 cm^{-1} and peaks from C=O at 1735 cm^{-1}. The oxygen in rGO is mostly bound to edge carbon atoms but some oxygen groups on the planar surface of sheets are also not completely removed by thermal reduction. It is known that complete removal of oxygen from rGO is not observed even after heating at very high temperatures. The relatively mild exfoliation temperature used in our study results in C/O=5-6. Oxidation of the rGO is reflected in FTIR spectra by the strong increase of C=O

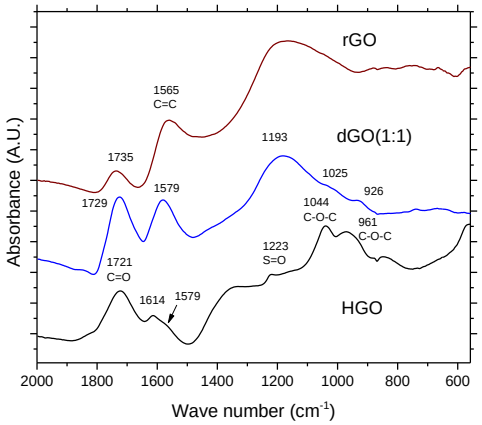

Figure 8. FTIR spectra of HGO, rGO produced by explosive exfoliation of this HGO and dGO (1:1) prepared by Hummers oxidation of rGO. Spectra recorded using ATR under vacuum conditions.

peak which also downshifts to 1729 cm^{-1}, more similar to the position of C=O peak in HGO. Position of C=C peak shifted from 1565 cm^{-1} in rGO to 1579 cm^{-1} of dGO (1:1), also more similar to standard HGO. However, the FTIR spectra provide clear evidence that Hummers oxidation of rGO results in synthesis of a material rather different compared to HGO. The peaks typically assigned to C-O-C and C-OH are rather weak in the spectra of dGO reflecting the extremely defect nature of this material and the absence of sufficient planar surface for these functional groups. In fact, the spectra of dGO exhibit some features similar to rGO and some features similar to HGO in FTIR spectra. It is known that the choice of precursor carbon material strongly affects the properties of GO.

3.2. Sorption properties of dGO.

Sorption of methylene blue. It is known that GO shows a high sorption capacity for methylene blue (MB). Moreover, sorption of MB was used in several studies for the evaluation of surface area accessible for GO in aqueous solutions.[16, 17] Therefore, we performed a rapid test to verify our initial assumption that the defect structure improves sorption properties of dGO. Indeed, the dGO sorption of methylene blue was found to be significantly enhanced compared to standard HGO. As a reference we tested also sorption of MB by BGO powder. As expected from our earlier studies, the more defect nature of HGO as compared to BGO results in twice higher amount of adsorbed MB (428 mg/g and 184 mg/g respectively). The sorption of MB by dGO is 879 mg/g, more than twice higher compared to standard HGO. Graphite oxides are known to exhibit a rather small surface area by gas sorption but significant surface area in water solutions.[17] The difference is explained by the effect of swelling. The nitrogen gas molecules do not penetrate between GO layers but the interlayer distance expands significantly due to intercalation of liquid water. Swelling of GO structure provides the possibility for dissolved molecules to enter interlayers of GO and to be adsorbed in significant amounts.

The gravimetric amounts of adsorbed MB are often recalculated into effective surface area values, as in the Table 2.[16, 60] Using this method the dGO shows a MB sorption surface area about 50% higher compared to the reference sample of porous carbon with BET (N_2) of ~2000 m^2/g. However, our results indicate that the estimation of surface area using MB needs to be treated with caution, as it is obviously dependent on the amount of defects in GO. Both HGO and BGO are swelling well thus providing very similar surface area in liquid water but the sorption of MB is rather different (Table 2). The difference in defect state is also likely to

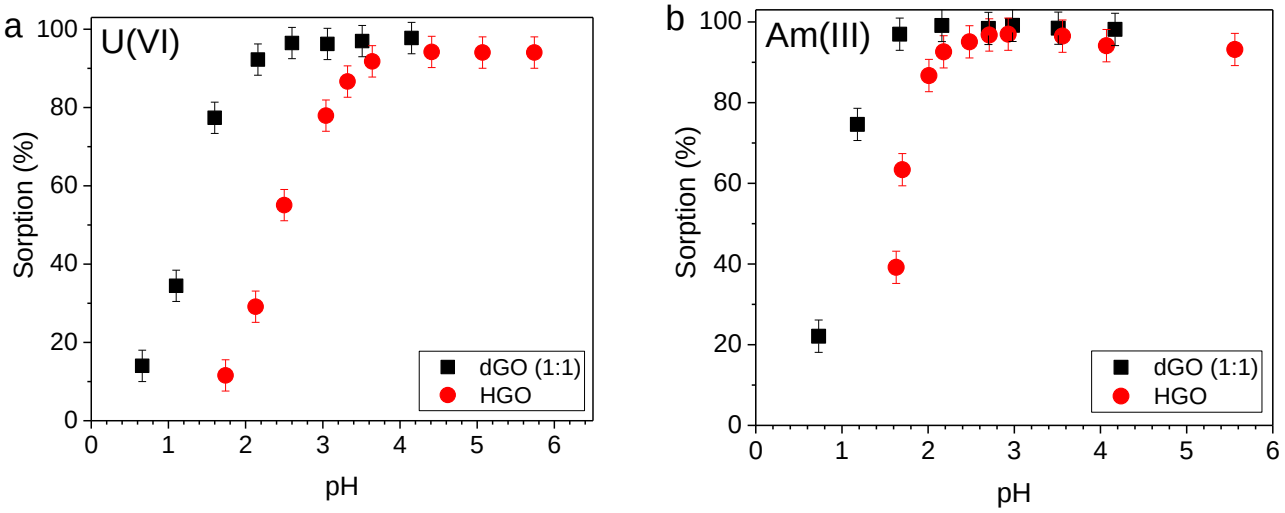

Figure 9. pH sorption edges for (a) – U(VI) and (b) – Am(III) onto dGO (1:1) and initial HGO. ([Am(III)]=6·10^{-10} M, [U(VI)]=2·10^{-7} M).

be a reason for rather strong spread in reported gravimetric values for MB sorption by GO in literature, typically 250-450 mg/g[60, 61] but with some reports up to ~700 mg/g.[62]

Sorption of radionuclides. Sorption of U(VI) and Am(III)/Eu(III) was tested for dGO and standard HGO. In agreement with our expectations the dGO (1:1) demonstrated a higher sorption ability for both U(VI) and Am(III) over the entire range of pH (Figure 9). The largest difference in sorption is observed at very low pH conditions. The pH value at 50% of sorption (pH50) is smaller for dGO(1:1) by 1.1 unit in case of U(VI), while for Am(III) it is 0.65 unit.

The enhanced sorption properties of dGO are attributed to the higher concentration of carboxyl groups compared to the HGO. Therefore, the sorption isotherm of radionuclides was used to estimate the amount of functional groups. The isotherms were firstly fitted by Langmuir model: $C_{sorb} = Q_{max} \cdot K_{La} \cdot C_{sol} / (1 + K_{La} C_{sol})$, where C_{sorb} is the equilibrium concentration of adsorbed radionuclides, C_{sol} is the equilibrium concentration of radionuclides in aqueous solution, Q_{max} is the maximum sorption capacity, K_{La} is a constant. According to the fit of experimental data (Table 3) the sorption capacity of dGO is significantly higher than of HGO – c.a. 15 times for U(VI) and c.a. 2 times for Am(III).

Comparing the sorption capacities determined from the Langmuir formalism for different experimental conditions is hardly possible. There are a lot of factors that influence sorption capacity, most importantly pH value and cation type. In particular, pH value of the sorption isotherm has a drastic effect on sorption ca-

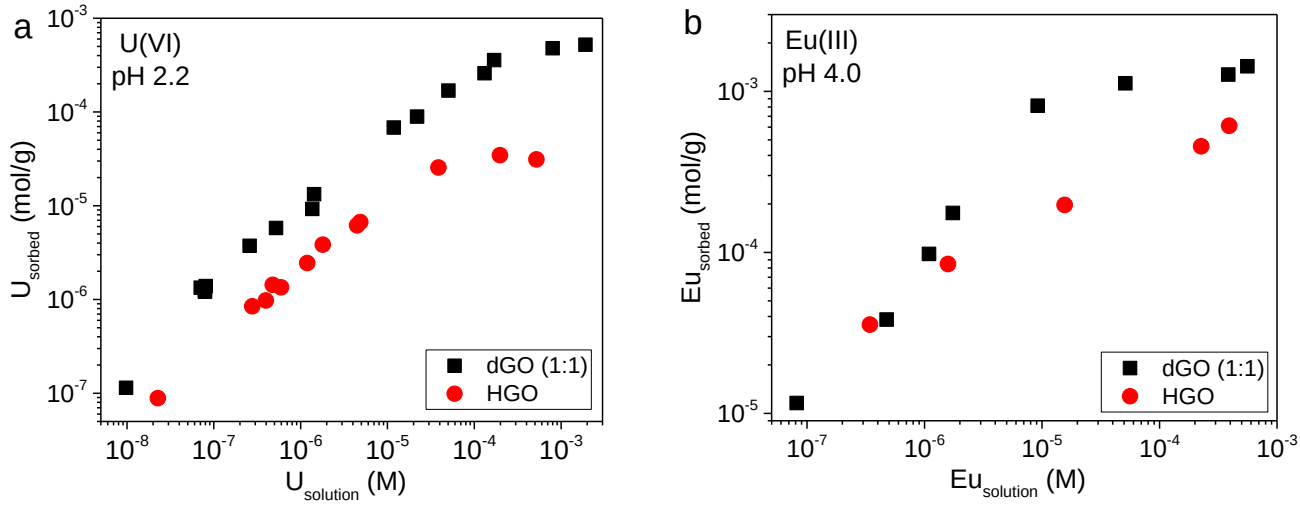

Figure 10. Sorption isotherms of radionuclides (a) – U(VI) and (b) Eu(III) onto HGO and dGO (1:1).

Table 3. Sorption capacity of the studied samples calculated by applying Langmuir model

Sample	Maximum sorption capacity Q_{max}, μmol/g	
	U(VI) at pH 2.2	Eu(III) at pH 4.0
HGO	35 ± 1	597 ± 58
dGO (1:1)	551 ± 12	1367 ± 50

pacity of GO as demonstrated in our earlier studies.[1]

A more sophisticated approach to describe sorption reaction is surface complexation modelling (SCM), assuming the sorption process as an exchange with a proton in the following reaction:

≡SOH + Cat^{n+} ⇆ ≡SO$Cat^{(n-1)+}$ + H^+, where ≡SOH – functional group on the surface.

This concept has found wide application for describing sorption of cations by different minerals.[63, 64] This approach was applied also to GO systems by some authors.[21, 23, 24, 26] However, even in the case of standard GO, this approach can be quite controversial due to the variety of functional groups found in GO. At least 5-7 oxygen functional groups are described in a standard structural model of GO[44], making modeling difficult and ambiguous. Moreover, the concentrations of functional groups in refs [21, 23, 24, 26] were determined by potentiometric titration. However, because of the complex structure of GO, not all functional groups that interact with H^+ may interact with other cations.

In the present study dGO samples contain predominantly carboxyl groups. Therefore, we performed SCM assuming that interaction occurs with a single averaged type of sorption sites. This assumption also supports the sorption isotherm shape where only one plateau is reached. In addition, unlike other works, we performed simultaneous fitting of all sorption data for Am(III)/Eu(III) and U(VI) (two pH-curve and two isotherms). A non-electrostatic model (NEM) was used for the modelling assuming that sorption occurs inside of hole defects on the graphene planes. We tested both formation of mono- and poly-dentate complexes onto the dGO surface. The better results were found using the concept of monodentate complex formation, Table 4.

Table 4. Parameters of optimization sorption data using SCM approach

	log*K*
≡SOH ⇆ ≡SO^- + H^+,	-4*
≡SOH + UO_2^{2+} ⇆ ≡SOUO_2^+ + H^+	2.35
≡SOH + Am^{3+} ⇆ ≡SOAm^{2+} + H^+	3.60
≡SOH + Eu^{3+} ⇆ ≡SOEu^{2+} + H^+	2.20
[≡SOH], mol/g	$7 \cdot 10^{-4}$

*was fixed [25]

The fit of the experimental data is adequate (Figure S2 in SI). The concentration of surface carboxyl groups was calculated as $7 \cdot 10^{-4}$ mol/g; that is 3.3 times higher than for standard GO in Xie and Powell work.[25] This result confirms that the defect nature of re-oxidized rGO with increased number of carboxylic groups is favorable for sorption. The interaction of radionuclides with GO occurs through complexation with carboxyl groups. Therefore the linear free energy relationship (LFER) between constants of interaction of radionuclides with simple carboxylic acids and GO should take place. In the present work we found that the sorption constant of Am(III), Eu(III) and U(VI) onto dGO is in a perfect linear correlation with the complexation constants with the acetate-ion (Figure S3 in SI).

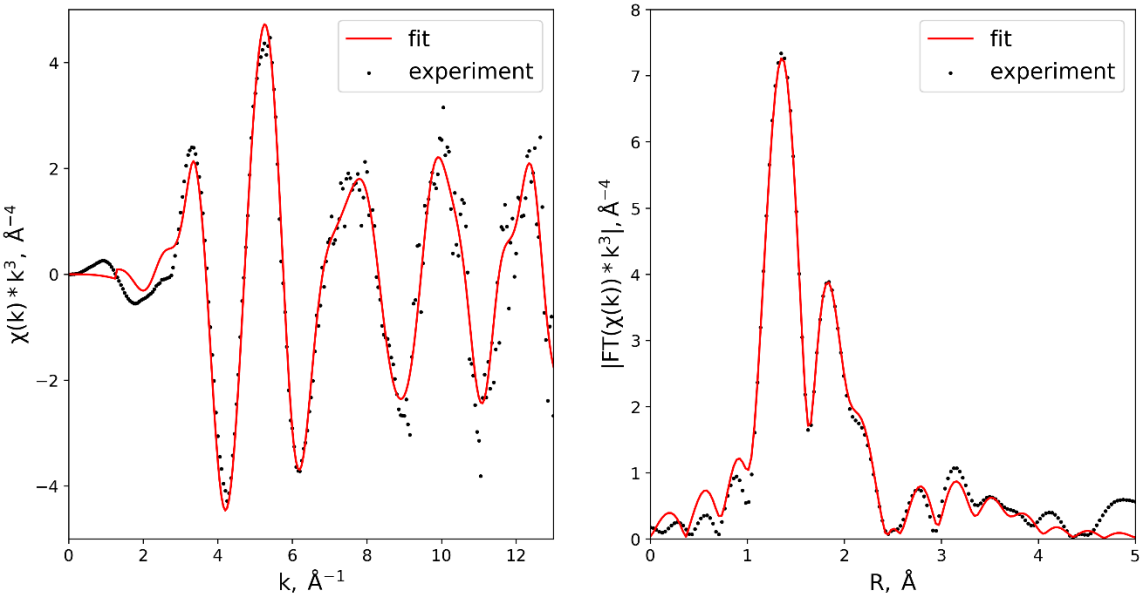

Figure 11 EXAFS spectra of U(VI) sorbed onto dGO(1:1): (a) – oscillation part of the EXAFS spectra, (b) – absolute values of Fourier transformations of the spectra. Dots represent the experimental data; lines are the fitting of the spectra.

Table 5. Structural parameters around uranium and GO samples derived from EXAFS analyses.

Sample		CN	R, Å	σ, Å²	ΔE, eV	
U(VI) + dGO (1:1)	U-O	2.0*	1.77	0.002	6.2	R-factor=0.005 R-range=1.1-4.0 Å k-range=3.0-13.0 Å^{-1}
	U-O	1.6	2.26	0.002		
	U-O	4.4	2.41	0.006		
	U-C	1.7	2.94	0.003		
	U-C	4.8	3.81	0.003		
	U-C	4.5	4.00	0.003		
U(VI) + HGO Ref.[2]	U-O	2.0*	1.75	0.001	2.2	R-factor = 0.002
	U-O	2.3	2.22	0.002		
	U-O	4.1	2.39	0.003		
	U-C	0.6	2.68	0.002		
	U-C	2.6	2.91	0.002		
	U-C	4.1	3.76	0.003		
	U-C	3.7	3.95	0.003		

To clarify the mechanism of radionuclide sorption by dGO we recorded EXAFS spectra after equilibration with cations. Analysis of the EXAFS spectra allows to make some conclusions on the local atomic environment of sorbed uranium.

Fitted experimental EXAFS spectra of U(VI) adsorbed by dGO (1:1) are presented in Figure 11 with corresponding structural parameters listed in Table 5. The EXAFS spectrum is rather similar to those for U(VI) on reference HGO suggesting a similar mechanism of sorption.[2] In U(VI) spectra, the first peak of the Fourier transform at 1.3-1.4 Å is the U-O shell and can be fitted with two axial uranyl oxygen atoms. The next peak corresponds to equatorial oxygen atoms and is fitted by two subshells with resulting coordination numbers of 2.26 and 2.41. The latter subshell corresponds to U-C interactions. Analysis of EXAFS spectra demonstrates that dGO material sorbs U(VI) with the exact same mechanism as the reference HGO, with carboxylic groups

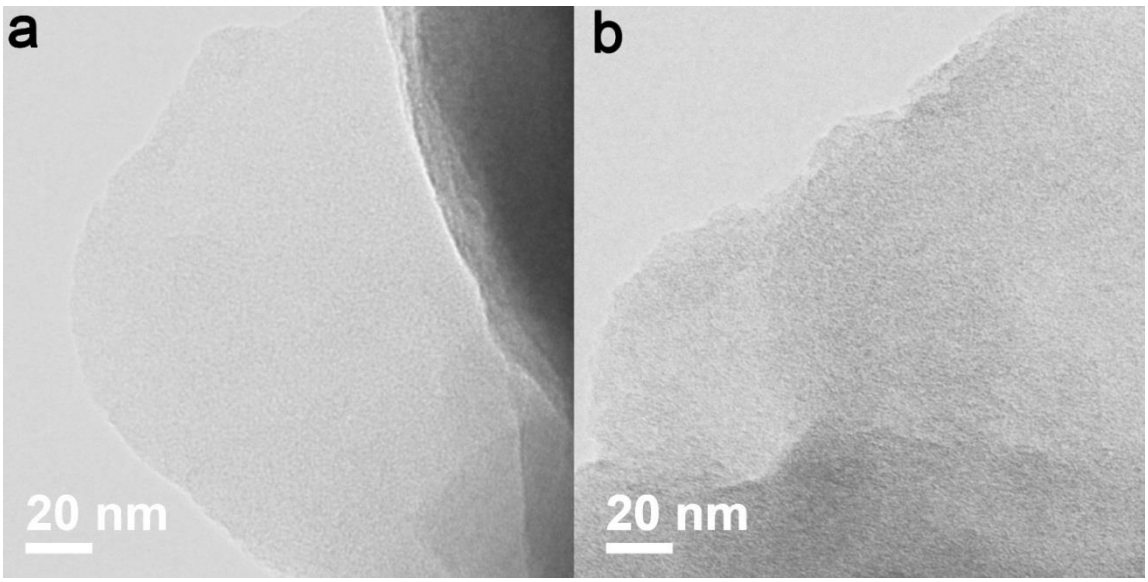

Figure 12. HRTEM image recorded from a) precursor dGO (1:1) and b) dGO(1:1) with adsorbed U(VI).

dominating the GO-cation interaction.

Additional evidence for the suggested mechanism of U(VI) sorption by dGO was obtained using High Resolution Transmission Electron Microscopy (HRTEM), Figure 12**.** Heavy atoms provide higher contrast in HRTEM and are relatively easy for imaging. However, images of dGO sample with sorbed U(VI) demonstrate the absence of clustering, formation of nanoparticles or extra concentration of uranium along the edges of flakes. In STEM regime the images also show that uranium is distributed homogeneously over the whole surface of dGO flakes. (Figure S4 in SI). The data suggest that U(VI) is bound to structural defects in GO sheets which are rather small in size, below the resolution of the images and homogeneously distributed over the whole area of flakes. According to our previous results based on EXAFS and modelling the main sorption sites in HGO for the binding of radionuclides are carboxylic groups on the inside edges of small ~ 1 nm size holes.[2] HRTEM images are in agreement with the suggested mechanism, showing a homogeneous distribution of uranium over the entire surface of dGO flakes.

Further confirmation of the similarity of the sorption mechanisms in dGO and standard HGO comes from HERFD-XANES measured at the Uranium M4 edge, which probes directly the f-orbitals through $3d_{3/2} \rightarrow 5f_{5/2}$ electronic transitions. The spectra measured on U(VI) sorbed onto HGO and dGO are shown in Figure 13. The spectra show the characteristic profile of the uranyl ion, with three well-separated peaks, which have been assigned to transition into the nonbonding $5f\delta_u$ and $5f\phi_u$, antibonding $5f\pi_u$*, and antibonding $5f\sigma_u$* molecular orbitals.[65] Aside from a small decrease in the intensity of the second peak in dGO compared with HGO the spectra are almost identical, indicative of a very similar local coordination environment in the two materials. In particular, the fact that the third peak is unchanged in energy position is a strong indication that the short U-O axial bonds are identical. Indeed, as the M4 HERFD probes directly the anti-bonding molecular orbitals of uranyl, this measurement is extremely sensitive to structural changes.

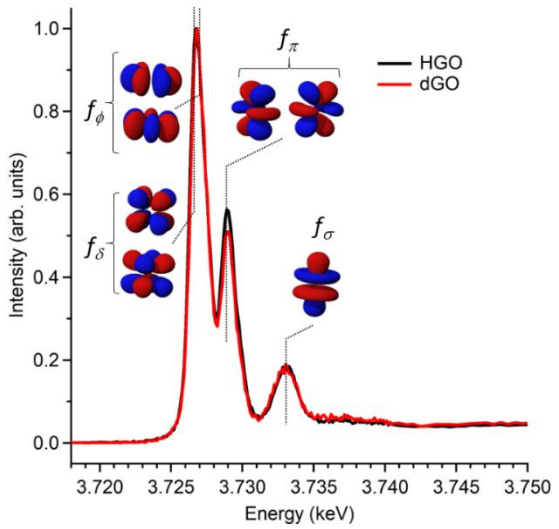

Figure 13. U M4 edge HERFD spectra of U(VI) sorbed on HGO and dGO (1:1). The three peaks correspond to transitions to the unoccupied molecular orbitals with U f character. Drawings of the f-orbitals involved in each transition are shown according to ref. [65]

Previous M4 HERFD measurements of uranyl in lithium borate glasses show that a 0.06 Å change of the bond length can result in a shift of the third peak (fσ) by as much as 1 eV.[66] A small shift can be recognized in HERFD-XANESspectra of U(VI) sorbed onto GO synthesized using three different methods: Hummers, Tour and Brodie (Figure S5 in SI) thus confirming the high sensitivity of this method to elongation of bond length. These three types of GO were characterized in detail in our previous study.[2] A small 0.01 Å elongation of the uranyl bond was found for BGO material using EXAFS[2] and indeed the third peak in M4 edge spectrum shows a shift of 0.7 eV to lower energy. An increase of the U-O axial bond distance results in energetic stabilization of the $5f\sigma_u$* orbital which, based on multiplet calculations (Figure S6 in SI), shifts the third peak to lower energies, in agreement with the experimental observations. The small intensity decrease of the second peak in dGO spectra indicates some differences in the local environment of U(VI). However the effect is minor and might be related to the equatorial U-O bonds, whose effect on the local electronic structure is weak.

Summarizing the data presented above, the mechanism of uranyl sorption by dGO is essentially the same as in standard HGO, which has a higher number of defects compared to BGO. This result confirms that material obtained by Hummers oxidation of rGO is also graphene oxide with all major properties typical for standard HGO but with a significant increase in the number of defects, which provides the 15-fold increase of uranyl sorption. It is a non-trivial result considering that the oxidation of defect-rich rGO is likely to result in formation of a variety of defects, e.g. holes of different diameter, edges of different shape etc. A relatively large overall number of carboxylic groups around the flake edges is also expected due to small flake size of dGO. However, uranyl cations are sorbed on dGO by a mechanism remarkably similar to standard HGO. The spectra shown in Figures 11, 13 show no new spectral features which could indicate appearance of abundant sites with different mechanism of sorption. No increased concentration of uranium is also found on HRTEM images on the edges of GO flakes (Figure 12).

Therefore, we suggest that only very specific sorption sites related to carboxylic groups on small holes in GO sheets (as in standard HGO[2]) are responsible for most of the uranyl sorption. Many other defect types which are inevitably formed in process of dGO synthesis do not contribute to the sorption of uranyl and remain unoccupied. This interpretation of data is confirmed by the fact that the number of carboxyl groups determined using XPS is about 10 times higher compared to the molar concentration of sorbed uranium cations. Therefore, only about 10% of carboxylic groups are providing sorp-

tion sites for uranyl while the rest are in defects or flake edges remain not suitable for uranyl sorption.

4. CONCLUSIONS

In conclusion, extremely defect-rich GO was prepared using Hummers oxidation of rGO and tested for sorption of several radionuclides. Following our earlier fundamental study of radionuclides binding to different types of GO, carboxylic groups located on the edges of small holes are responsible for the sorption of e.g. uranyl cations. The dGO material was therefore designed specifically with the aim to increase the number of defects. The precursor rGO was intentionally prepared using explosive exfoliation at conditions which provide the maximal number of defects. Further oxidation of highly dispersed and defect rGO result in the formation of material which has about 10 fold higher number of carboxylic groups compared to standard HGO and an unusually low number of oxygen groups which are typically found on the planar surface of GO sheets. Simple analysis of XPS data allows to estimate that about 10% of all carbon atoms in dGO are located on the edges of flakes or inner edges of holes, thus forming an extremely defect structure.

In agreement with our expectation the dGO material showed 15-fold increase in sorption of U(VI) and two-fold increase in sorption of Am(III). As revealed by high resolution microscopy, the uranyl cations are homogeneously distributed over the dGO flakes, showing no aggregation. Analysis of electron and synchrotron-based spectroscopy data – EXAFS and HERFD-XANES allows to conclude that the enhanced sorption of uranyl by dGO is related to the same type of defects as in standard HGO. According to modeling results, uranyl cations are bound to carboxylic groups located inside of small holes in dGO and HGO structure. However, the overall number of these defects is higher in dGO which results in a significantly improved sorption capacity which can be useful in many applications related to treatment of toxic and radioactive wastes.

ASSOCIATED CONTENT

The supporting information is available free of charge via the Internet at http://pubs.acs.org.

AUTHOR INFORMATION

Corresponding Authors

Alexandr Talyzin: alexandr.talyzin@umu.se
Stepan Kalmykov: stepan@radio.chem.msu.ru

Author Contributions

The manuscript was written through contributions of all authors. / All authors have given approval to the final version of the manuscript. / ‡These authors contributed equally. (match statement to author names with a symbol)

ACKNOWLEDGMENT

N.B and A.T acknowledge funding from the European Union's Horizon 2020 research and innovation program under grant agreement No785219 and No 881603. Support from Swedish Research Council grant (no. 2017-04173) is also acknowledged. We also acknowledge Vibrational Spectroscopy Platform of Umeå University and A. Shchukarev for support with XPS test. The experimental studies were partially performed on equipment acquired with funding by the Lomonosov Moscow State University Development Program. Authors acknowledge help of J. Rothe, K. Dardenne, A. Beck, T. Prussman, T. Vitova at CAT-ACT beamline of KARA during the HERFD-XANES experiment at the U M_4 edge. We would like to thank S.Weiss from the HZDR safety group for his help in handling radioactive samples for HERFD-XANES experiment. L.A, S. B and K.O.K. acknowledge the support from the European Research Council (ERC) (grant agreement No 759696) (HERFD-XANES experiment). A.S.K, and S.N.K acknowledge support by the Russian Ministry of Science and Education under grant № 075-15-2019-1891 (sorption experiments on radionuclides).

REFERENCES

1. A. Y. Romanchuk, A. S. Slesarev, S. N. Kalmykov, D. V. Kosynkin and J. M. Tour, *Phys Chem Chem Phys*, 2013, **15**, 2321-2327.
2. A. S. Kuzenkova, A. Y. Romanchuk, A. L. Trigub, K. I. Maslakov, A. V. Egorov, L. Amidani, C. Kittrell, K. O. Kvashnina, J. M. Tour, A. V. Talyzin and S. N. Kalmykov, *Carbon*, 2020, **158**, 291-302.
3. A. Y. Romanchuk, A. S. Kuzenkova, A. S. Slesarev, J. M. Tour and S. N. Kalmykov, *Solvent Extr Ion Exc*, 2016, **34**, 594-602.
4. E. H. Borai, R. Harjula, L. Malinen and A. Paajanen, *J Hazard Mater*, 2009, **172**, 416-422.
5. M. Pansini, *Miner Deposita*, 1996, **31**, 563-575.
6. L. De Windt, D. Pellegrini and J. van der Lee, *J Contam Hydrol*, 2004, **68**, 165-182.
7. K. F. Li and X. Y. Pang, *Cement Concrete Res*, 2014, **65**, 52-57.
8. A. A. M. Abdel-Karim, A. A. Zaki, W. Elwan, M. R. El-Naggar and M. M. Gouda, *Appl Clay Sci*, 2016, **132**, 391-401.
9. A. W. Miller and Y. F. Wang, *Environ Sci Technol*, 2012, **46**, 1981-1994.
10. M. H. Bradbury and B. Baeyens, *Geochim Cosmochim Ac*, 2005, **69**, 875-892.
11. C. B. Durrant, J. D. Begg, A. B. Kersting and M. Zavarin, *Sci Total Environ*, 2018, **610**, 511-520.
12. M. R. Mahmoud, G. E. S. El-Deen and M. A. Soliman, *Ann Nucl Energy*, 2014, **72**, 134-144.
13. Y. F. Wang, H. Z. Gao, R. Yeredla, H. F. Xu and M. Abrecht, *J Colloid Interf Sci*, 2007, **305**, 209-217.
14. N. Savage and M. S. Diallo, *J Nanopart Res*, 2005, **7**, 331-342.
15. Y. A. Mackeyev, J. W. Marks, M. G. Rosenblum and L. J. Wilson, *J Phys Chem B*, 2005, **109**, 5482-5484.
16. P. Montes-Navajas, N. G. Asenjo, R. Santamaria, R. Menendez, A. Corma and H. Garcia, *Langmuir*, 2013, **29**, 13443-13448.
17. H. P. Boehm, A. Clauss, G. Fischer and C. Hofmann, *Proc. 5th Conf. on Carbon (Oxford: Pergamon)* 1962, 73-80.
18. J. H. Sun, F. Morales-Lara, A. Klechikov, A. V. Talyzin, I. A. Baburin, G. Seifert, F. Cardano, M. Baldrighi, M. Frasconi and S. Giordani, *Carbon*, 2017, **120**, 145-156.
19. L. Q. Tan, S. Wang, W. G. Du and T. Hu, *Chem Eng J*, 2016, **292**, 92-97.

20. C. L. Wang, Y. Li and C. L. Liu, *J Radioanal Nucl Ch*, 2015, **304**, 1017-1025.
21. Y. Xie, E. M. Helvenston, L. C. Shillller-Nickles and B. A. Powell, *Environ Sci Technol*, 2016, **50**, 1821-1827.
22. Z. J. Li, F. Chen, L. Y. Yuan, Y. L. Liu, Y. L. Zhao, Z. F. Chai and W. Q. Shi, *Chem Eng J*, 2012, **210**, 539-546.
23. T. A. Duster, J. E. S. Szymanowski and J. B. Fein, *Environ Sci Technol*, 2017, **51**, 8510-8518.
24. D. G. Gu and J. B. Fein, *Colloid Surface A*, 2015, **481**, 319-327.
25. Y. Xie and B. A. Powell, *Acs Appl Mater Inter*, 2018, **10**, 32086-32092.
26. T. Hu, S. J. Ding and H. J. Deng, *Chem Eng J*, 2016, **289**, 270-276.
27. R. R. Amirov, J. Shayimova, Z. Nasirova and A. M. Dimiev, *Carbon*, 2017, **116**, 356-365.
28. W. S. Hummers and R. E. Offeman, *J Am Chem Soc*, 1958, **80**, 1339-1339.
29. B. C. Brodie, *Philosophical Transactions of the Royal Society of London*, 1859, **149**, 249-259.
30. D. C. Marcano, D. V. Kosynkin, J. M. Berlin, A. Sinitskii, Z. Z. Sun, A. Slesarev, L. B. Alemany, W. Lu and J. M. Tour, *Acs Nano*, 2010, **4**, 4806-4814.
31. H. P. Boehm and W. Scholz, *Z Anorg Allg Chem*, 1965, **335**, 74-&.
32. S. You, S. M. Luzan, T. Szabo and A. V. Talyzin, *Carbon*, 2013, **52**, 171-180.
33. A. V. Talyzin, G. Mercier, A. Klechikov, M. Hedenstrom, D. Johnels, D. Wei, D. Cotton, A. Opitz and E. Moons, *Carbon*, 2017, **115**, 430-440.
34. A. V. Talyzin, A. Klechikov, M. Korobov, A. T. Rebrikova, N. V. Avramenko, M. F. Gholami, N. Severin and J. P. Rabe, *Nanoscale*, 2015, **7**, 12625-12630.
35. A. V. Talyzin, T. Hausmaninger, S. J. You and T. Szabo, *Nanoscale*, 2014, **6**, 272-281.
36. S. J. You, S. Luzan, J. C. Yu, B. Sundqvist and A. V. Talyzin, *J Phys Chem Lett*, 2012, **3**, 812-817.
37. P. Feicht, R. Siegel, H. Thurn, J. W. Neubauer, M. Seuss, T. Szabo, A. V. Talyzin, C. E. Halbig, S. Eigler, D. A. Kunz, A. Fery, G. Papastavrou, J. Senker and J. Breu, *Carbon*, 2017, **114**, 700-705.
38. M. V. Korobov, A. V. Talyzin, A. T. Rebrikova, E. A. Shilayeva, N. V. Avramenko, A. N. Gagarin and N. B. Ferapontov, *Carbon*, 2016, **102**, 297-303.
39. T. Szabo, O. Berkesi, P. Forgo, K. Josepovits, Y. Sanakis, D. Petridis and I. Dekany, *Chem Mater*, 2006, **18**, 2740-2749.
40. K. Krishnamoorthy, M. Veerapandian, K. Yun and S. J. Kim, *Carbon*, 2013, **53**, 38-49.
41. A. M. Dimiev, L. B. Alemany and J. M. Tour, *Acs Nano*, 2013, **7**, 576-588.
42. S. Kim, S. Zhou, Y. K. Hu, M. Acik, Y. J. Chabal, C. Berger, W. de Heer, A. Bongiorno and E. Riedo, *Nat Mater*, 2012, **11**, 544-549.
43. A. Iakunkov, J. H. Sun, A. Rebrikova, M. Korobov, A. Klechikov, A. Vorobiev, N. Boulanger and A. V. Talyzin, *J Mater Chem A*, 2019, **7**, 11331-11337.
44. A. Lerf, H. Y. He, M. Forster and J. Klinowski, *J Phys Chem B*, 1998, **102**, 4477-4482.
45. K. Erickson, R. Erni, Z. Lee, N. Alem, W. Gannett and A. Zettl, *Adv Mater*, 2010, **22**, 4467-4472.
46. Z. L. Liu, K. Norgaard, M. H. Overgaard, M. Ceccato, D. M. A. Mackenzie, N. Stenger, S. L. S. Stipp and T. Hassenkam, *Carbon*, 2018, **127**, 141-148.
47. A. Gogoi, A. Koneru and K. A. Reddy, *Nanoscale Adv*, 2019, **1**, 3023-3035.
48. P. Feicht and S. Eigler, *Chemnanomat*, 2018, **4**, 244-252.
49. R. R. Amirov, J. Shayimova, Z. Nasirova, A. Solodov and A. M. Dimiev, *Phys Chem Chem Phys*, 2018, **20**, 2320-2329.
50. M. Cheng, R. Yang, L. C. Zhang, Z. W. Shi, W. Yang, D. M. Wang, G. B. Xie, D. X. Shi and G. Y. Zhang, *Carbon*, 2012, **50**, 2581-2587.
51. S. Eigler, C. Dotzer and A. Hirsch, *Carbon*, 2012, **50**, 3666-3673.
52. M. H. Overgaard, M. Kuhnel, R. Hvidsten, S. V. Petersen, T. Vosch, K. Norgaard and B. W. Laursen, *Adv Mater Technol-Us*, 2017, **2**.
53. A. G. Klechikov, G. Mercier, P. Merino, S. Blanco, C. Merino and A. V. Talyzin, *Micropor Mesopor Mat*, 2015, **210**, 46-51.
54. M. Newville, *J Synchrotron Radiat*, 2001, **8**, 96-100.
55. A. Zimina, K. Dardenne, M. A. Denecke, D. E. Doronkin, E. Huttel, H. Lichtenberg, S. Mangold, T. Pruessmann, J. Rothe, T. Spangenberg, R. Steininger, T. Vitova, H. Geckeis and J. D. Grunwaldt, *Rev Sci Instrum*, 2017, **88**.
56. J. Rothe, M. Altmaier, R. Dagan, K. Dardenne, D. Fellhauer, X. Gaona, E. G. R. Corrales, M. Herm, K. O. Kvashnina, V. Metz, I. Pidchenko, D. Schild, T. Vitova and H. Geckeis, *Geosciences*, 2019, **9**.
57. I. A. Baburin, A. Klechikov, G. Mercier, A. V. Talyzin and G. Seifert, *Int J Hydrogen Energ*, 2015, **40**, 6594–6599.
58. A. Klechikov, J. H. Sun, G. Z. Hu, M. B. Zheng, T. Wagberg and A. V. Talyzin, *Micropor Mesopor Mat*, 2017, **250**, 27-34.
59. A. V. Talyzin, T. Szabo, I. Dekany, F. Langenhorst, P. S. Sokolov and V. L. Solozhenko, *J Phys Chem C*, 2009, **113**, 11279-11284.
60. H. P. Boehm, A. Clauss, G. O. Fischer and U. Hofmann, *Z Anorg Allg Chem*, 1962, **316**, 119-127.
61. P. Bradder, S. K. Ling, S. B. Wang and S. M. Liu, *J Chem Eng Data*, 2011, **56**, 138-141.
62. S. T. Yang, S. Chen, Y. L. Chang, A. N. Cao, Y. F. Liu and H. F. Wang, *J Colloid Interf Sci*, 2011, **359**, 24-29.
63. V. Brendler, A. Vahle, T. Arnold, G. Bernhard and T. Fanghanel, *J Contam Hydrol*, 2003, **61**, 281-291.
64. T. E. Payne, V. Brendler, M. Ochs, B. Baeyens, P. L. Brown, J. A. Davis, C. Ekberg, D. A. Kulik, J. Lutzenkirchen, T. Missana, Y. Tachi, L. R. Van Loon and S. Altmann, *Environ Modell Softw*, 2013, **42**, 143-156.
65. T. Vitova, J. C. Green, R. G. Denning, M. Loble, K. Kvashnina, J. J. Kas, K. Jorissen, J. J. Rehr, T. Malcherek and M. A. Denecke, *Inorg Chem*, 2015, **54**, 174-182.
66. M. O. J. Y. Hunault, G. Lelong, L. Cormier, L. Galoisy, P. L. Solari and G. Calas, *Inorg Chem*, 2019, **58**, 6858-6865.
67. M. Retegan, 2019.
68. M. W. Haverkort, M. Zwierzycki and O. K. Andersen, *Phys Rev B*, 2012, **85**.